σ-IASI-β: A HYPERFAST RADIATIVE TRANSFER CODE TO RETRIEVE SURFACE AND ATMOSPHERIC GEOPHYSICAL PARAMETERS

Giuseppe Grieco, Carmine Serio, and Guido Masiello

University of Basilicata, School of Engineering, Potenza, Italy;
giuseppe.grieco(at)gmail.com, {carmine.serio / guido.masiello }(at)unibas.it

ABSTRACT

This paper describes an improved, faster, implementation of the σ-IASI model, with a new parameterization of radiative transfer in cloudy atmosphere. The model can compute up and/or downwelling spectral radiances, emitted from the Earth's system and their analytical Jacobians with respect to a set of geophysical parameters and the water vapour and carbon dioxide continua absorbing coefficients. The paper presents also its software implementation and a retrieval exercise of the tropospheric content of CO_2, CO, N_2O and CH_4 on the Mediterranean Sea. The content of the gases is compared with the ground-based measurements of the Global Atmosphere Watch network. The innovation introduced in the model is the down-sampling of the look-up table by means of a spectral averaging of the layer optical depths on bins of 10^{-2} cm^{-1} width before they are parameterized as a low order polynomial of temperature and, only for water vapour, of water vapour concentration itself to take into account the self-broadening effect.

The down-sampling of the look-up table is responsible for an additional speed-up which makes the code useful for almost real time retrieval applications and thus useful for operational purposes.

This code is a powerful tool also to check the validity of the molecular spectroscopic parameters. It is an evolution of the well-known code σ-IASI. It has been developed in the context of the Infrared Atmospheric Sounding Interferometer (IASI) of the European Space Agency EUMETSAT, but it is well suited for every nadir viewing satellite, airplane sensor or ground-based sensor with a sampling rate in the range 0.1-2 cm^{-1}.

INTRODUCTION

Humidity and temperature have been identified as major variables in assessing climate change and they play a fundamental role in Earth's energy and water cycle processes. An accurate knowledge of also the minor and trace gases plays a fundamental role in the comprehension of the climate. It is now recognized that the current spectral resolution of modern hyperspectral sensors (resolution ≈0.5 cm^{-1}) meets the specifications issued by the World Meteorological Organization (WMO) on accuracy needed to improve weather forecasts (temperature with an average error of 1 K; humidity with an average error of 10-20%; vertical resolution of 1 km, at least in the lower troposphere).

Among these instruments are the American Advanced Infrared Radiometer Sounder (AIRS) (1) which flies on board the polar orbiting satellite platform AQUA issued by NASA and the European Infrared Atmospheric Sounding Interferometer (IASI) (2) which flies on board the polar orbiting satellite platform MetOp issued by EUMETSAT.

The accuracy of our knowledge of the thermodynamic state of the atmosphere and the minor and trace gases depends firstly on the quality of the observations, but also on the strategy adopted for the retrieval of the geophysical parameters. Physical based inversion methods have largely demonstrated to be the most accurate (3) even if, on the other hand, they are not competitive from a time performance point of view. This aspect poses a strong limit to the full exploitation of all the available observations. To have an idea of the burden of the available high spectral resolution observations, consider that IASI is able to measure 120 radiance spectra every 8 seconds and this burden will further increase with the Meteosat Third Generation mission. Consequently, an inverse

DOI: 10.12760/01-2013-2-07

tool should be able to retrieve the thermodynamic state of the atmosphere and minor and trace gases in less than one second.

The core of an inverse tool is the direct radiative transfer model and it is also the most time-consuming part of the process. This is the reason why so many different strategies have been developed in order to approximate the computation of the radiance spectrum and its derivatives with respect to the geophysical parameters.

This paper fully describes a hyper-fast monochromatic radiative transfer model designed for research and operational computation of either clear sky or cloudy spectral radiance, its analytical derivatives (Jacobians) with respect to a given set of geophysical parameters and the absorbing coefficients of the continua of H_2O and CO_2, and its software implementation. It is an evolution of the well-known σ-IASI code. It is based on a down-sampled look-up table of pre-computed optical depths and has been designed for every instrument which sounds the emitted spectrum of the Earth in the spectral range from 0 to 2800 cm^{-1} with a sampling rate between 0.1 and 2 cm^{-1} for nadir viewing satellites and airborne sensors and for ground-based sensors. The code is expected to provide the needed accurate forward model calculation for meteorological and climate application in order to retrieve the thermodynamic state of the atmosphere and the tropospheric concentration of trace and minor gases. Finally, it can be used in radiance closure studies to assess the consistency of the spectroscopic parameters (3).

An application of the code with the purpose of retrieving the tropospheric concentration of CO_2, CO, CH_4 and N_2O over the whole Mediterranean Sea for the month of July 2010 is presented and discussed. The retrieved values are then compared with the *in situ* ground-based measurements of the Global Atmosphere Watch network.

METHODS

Optical depth down-sampling methodology

The basic ingredients to compute the spectral radiance and its Jacobians with respect to the geophysical parameters are a) the thermodynamic state of the atmosphere and the vertical concentration profile of all the chemical species (atmospheric profile) and b) the monochromatic layer optical depth. The monochromatic layer optical depth depends itself on the atmospheric profile. The generation of the monochromatic layer optical depth is the most time-consuming part of the code. The basic idea to speed-up the code is to compute only once the layer optical depth and then store it in a suitable lookup table (4).

The innovation introduced here is the down-sampling of the layer optical depth lookup table.

The new down-sampled layer optical depth lookup table has been derived from the fine resolution layer optical depth lookup table whose computation is largely described in (4) and whose spectral resolution is 10^{-4} cm^{-1}.

For each species (*h*) we can define an equivalent optical depth $\chi^{(h)}_{<\nu>}$ that can be parameterized with respect to temperature (and with respect to water vapour mixing ratio for the only case of the water vapour to take into account the self-broadening effect (5)). With the symbols $\langle\cdot\rangle$ we indicate the average operation over the desired spectral range. This is what we mean by the coarse resolution layer optical depth lookup table (10^{-2} cm^{-1}).

Given that $q^{(h)}_j$ is the mass mixing ration of the (*h*)-th species and T_j is the physical temperature of the *j*-th atmospheric layer, the equivalent optical depth is:

$$\chi^{(h)}_{<\nu>,j} = q^{(h)}_j \left(c^{(h)}_{<\nu>,0j} + c^{(h)}_{<\nu>,1j} T_j + c^{(h)}_{<\nu>,2j} T_j^2 \right) \quad (1)$$

where the equivalent coefficients $c^{(h)}_{<\nu>,kj}$ with k = 0, 1, 2, are obtained by fitting the layer transmittance averaged over the coarse resolution

$$q_j^{(h)}\left(c_{<\nu>,0j}^{(h)} + c_{<\nu>,1j}^{(h)} T_j + c_{<\nu>,2j}^{(h)} T_j^2\right) = -\log\left(\left\langle \tau_{\nu,j}^{(h)} \right\rangle\right) = -\log\left[\left\langle \exp\left(-\chi_{\nu,j}^{(h)}\right)\right\rangle\right] \quad (2)$$

For upwelling radiance, the optical depth of the *j*-th layer may be written as:

$$\chi_j^{(h)} = -\log\left(\frac{\tau_{j-1}^{(h)}}{\tau_j^{(h)}}\right) \quad (3)$$

while for downwelling radiance it may be written as:

$$\chi_j^{(h)} = -\log\left(\frac{\tau_j^{*(h)}}{\tau_{j-1}^{*(h)}}\right) \quad (4)$$

Here, for the (*h*)-th chemical species $\tau_j^{(h)}$ is the transmittance of the atmosphere from the top of the *j*-th layer to the top of the atmosphere, while $\tau_j^{*(h)}$ represents the transmittance of the top of the *j*-th layer to the bottom of the atmosphere and therefore, they obey the relation

$$\tau_0^{(h)} = \tau_j^{(h)} \cdot \tau_j^{*(h)} \quad (5)$$

The discretization of the atmosphere and the average process introduce some errors; therefore, the correct computation of the layer optical depth depends on the observation point. For the upwelling case, the layer optical depth is computed recursively from the top to the bottom of the atmosphere, whilst the opposite happens for the downwelling case.

The monochromatic layer optical depth has been calculated by means of the Line By Line Radiative Transfer Model (LBLRTM) v12.1 (6) for a reference atmospheric state (US Standard Atmosphere 1962 (7)) plus eight evenly spaced temperatures (±10K; … ; ±40K). The required spectroscopic parameters have been extracted from the database HITRAN 2008 (8).

Retrieval methodology

The retrieval algorithm for the trace gases CO_2, CO, CH_4 and N_2O is based on the Fourier Transform Spectroscopy with Partially Scanned Interferogram technique (here-on FTS-PSI) and it uses the σ-IASI-β code as a subroutine.

The FTS-PSI has been applied in the recent past in order to retrieve the CO_2 columnar content and the vertical mixing ratio (VMR) of water vapour (9) and for an optimal spectral data reduction for the assimilation of spectral information in meteorological general circulation models (10).

We apply a parametric retrieval of the VMR trace gas profile making the following hypothesis:

$$q(p) = q_0(p)(1 + f_q) \quad (6)$$

where p is the atmospheric pressure (with the implicit dependence on the altitude), $q(p)$ is the VMR profile to be retrieved, $q_0(p)$ is a suitable first guess reference VMR profile coming from the climatology and f is the parameter to be retrieved.

In (11) the authors show that a parametric and a non-parametric approach for the retrieval of the N_2O tropospheric concentration are almost equivalent in terms of accuracy and degrees of freedom of the solution, the first one being faster. The retrieved quantity is representative of the tropospheric concentration of the gases. In fact, a) the sensitivity of the radiance to the trace gases concentration in the lowest layers of the atmosphere is very low, due to the poor thermal contrast between the sea surface and the lowest atmospheric layers and to the fact that the sea emissivity is very close to 1 (11) and b) the Jacobians do not have any sharp peak, all over their absorption spectral interval (we omit here for the sake of brevity) and it can be seen that most of the contribution to the total columnar content of the gas *Q* comes from the part of the atmosphere between 200 and 700-800 hPa.

Given that the final retrieved solution has just one degree of freedom, the only retrieved physical information concerns *Q*. It follows that the retrieved value *Q* is given by

$$Q = Q_0(1 + f_q) \tag{7}$$

where Q_0 is the total columnar content of the gas for the reference VMR profile.

The retrieval procedure for every trace gas goes through the following steps:

We produce a suitable first guess atmospheric state vector $\mathbf{v_0}$ coming from the simultaneous retrieval of T, T_s, water vapour and ozone by means of an optimal estimation retrieval algorithm as described in (3) and from climatology as far as trace gases are concerned.

We back-transform the observed radiance spectrum into the interferogram domain and select the proper optical path interval for the trace gas at hand, see (9) for details concerning the FTS-PSI retrieval technique.

We assume that the true state vector $\mathbf{v}$ is scaled with respect to $\mathbf{v_0}$:

$$\mathbf{v_i} = \mathbf{v_{0i}}(1 + f_i) \tag{8}$$

where $\mathbf{v_i}$ stands for the final atmospheric state vector concerning the geophysical parameter *i* to be retrieved and f_i is the parameter to be retrieved. Here, the index *i* refers to the trace gas object of the retrieval and to any potentially interfering parameter retrieved with the optimal estimation algorithm (T, T_s, water vapour and ozone).

We produce a least square regression of $\mathbf{f}$ (whose components are f_i) directly in the interferogram domain by means of the following relation

$$\mathbf{f} = \left(\mathbf{A}^t\mathbf{C}^{-1}\mathbf{A}\right)^{-1}\mathbf{A}^t\mathbf{C}^{-1}\Delta\mathbf{I} \tag{9}$$

where $\mathbf{C^{-1}}$ is the observational error covariance matrix in the interferogram domain, $\Delta\mathbf{I}$ is the difference between the interferogram concerning the observed radiance spectrum and the interferogram concerning the first guess solution and $\mathbf{A}$ is the matrix of the Jacobians of the geophysical parameters which have a non-negligible effect in the selected optical path interval multiplied by their initial guess state $\mathbf{v_0}$. All the potentially interfering parameters are expected to have a negligible variation, delimited by the precision of the optimal estimation retrieval. The intensity of this interfering effect is quantified by the index $\Delta_{\%}$ described later.

We estimate the accuracy of the method by computing the *a-posteriori* covariance matrix for the vector $\mathbf{f}$

$$\mathbf{S} = \left(\mathbf{A}^t\mathbf{C}^{-1}\mathbf{A}\right)^{-1} \tag{10}$$

From the error propagation law, we have that

$$\sigma_Q = \sigma_{f_q} Q_0 \tag{11}$$

where σ_Q is the estimated accuracy of the trace gas content Q, σ_{fq} is the precision of the retrieved parameter f_q and Q_0 is the reference columnar content of the trace gas.

We assess the relative weight of the interfering geophysical parameters on the trace gas content by means of the index $\Delta_{\%}$:

$$\Delta_{\%} = \sum_{i=1}^{N-1} \left|f_i\right| \cdot 100 \tag{12}$$

where the index $i \neq N$ stands for every interfering parameter. $\Delta_{\%}$ is an *ad-hoc* index which measures the deviation of the final state vector from the optimal estimated solution concerning the interfering parameters. It follows that if $\Delta_{\%}$ is high, the final solution is too far from the initial guess in respect of the interfering parameters previously retrieved, therefore the solution is not trustful. This deviation may be caused for example by a small cloud contamination. Concerning the problem at hand,

a suitable threshold value for $\Delta_{\%}$ is 10, otherwise the complete solution is rejected. $\Delta_{\%}$ may be considered also a by-product of this method to be used as an *a-posteriori* quality check of the optimal estimation retrieval.

It must be remarked that the final state **v** is a solution only in respect of the columnar content of the gas. Concerning the parameters retrieved at the first retrieval step by means of the optimal estimation algorithm, the solution does not change.

The estimated accuracy of this methodology is resumed in Table 1. It is referred to a single IASI pixel. The accuracy can be further improved by averaging with the neighbouring pixels. IASI instantaneously acquires a 4-pixel matrix which lies in a box of around 50 km side at nadir. Therefore, the estimated accuracy may be improved by a factor 2 given that the spatial resolution is decreased to about 50 km at nadir.

Table 1: Estimated accuracy of the tropospheric content of the trace gases.

Chemical Species	Estimated Accuracy
CO_2	1%
CO	<1%
N_2O	4-5%
CH_4	1.5%

RESULTS

The retrieval of the tropospheric content of the trace gases has been compared to the ground measurements of five Mediterranean stations of the Global Atmosphere Watch network and the data have been downloaded from the web site of the World Data Centre for Greenhouse Gases (http://ds.data.jma.go.jp/gmd/wdcgg/wdcgg.html). These stations are located in Begur (Spain), Finokalia (Greece), both owned by Laboratoire des Sciences du Climat et de l'Environnement de l'Institut Pierre Simone Laplace (LSCE/IPSL), Lampedusa (Italy), Sede Boker (Israel), both owned by Earth System Research Laboratory of the National Oceanic and Atmospheric Administration (ESRL/NOAA and another one in Lampedusa owned by the Italian National Agency for New Technologies, Energy and Sustainable Economic Development ENEA) and Cairo (Egypt), owned by the Egyptian Meteorological Authority (EMA). They span the entire Mediterranean basin. The first three stations lie at the seaside, whilst the last two are about 50 km and 150 km respectively from the coast. The last two stations have been selected, because they are the only stations available in the eastern Mediterranean basin. Figure 1 shows the location of the stations.

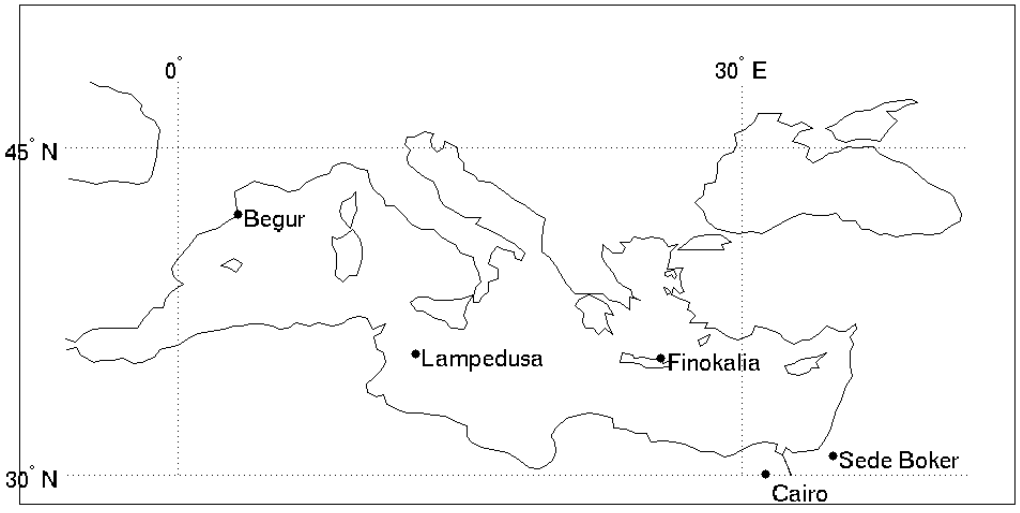

Figure 1: Location of the GAW stations.

Figure 2 shows the distribution of all available clear sky IASI measurements for the period of July 2010.

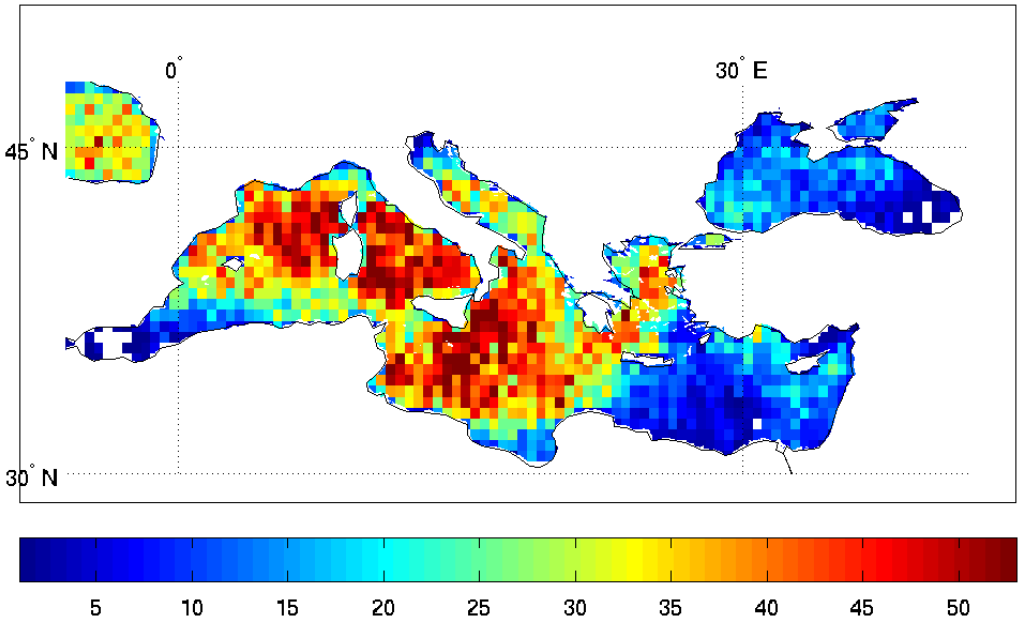

Figure 2: Spatial distribution of available IASI measurements in bins of 0.5° × 0.5° latitude/longitude.

The inhomogeneity of the distribution is due to the orbit characteristics of the satellite and to the cloud cover. We remark here that the platform is a polar orbiting satellite.

CO_2

Carbon dioxide has the largest radiative forcing (RF) among all the Greenhouse Gases (from now on GHG). Even if its radiative forcing power is lower than that of some other trace gases like N_2O, the dependence of our life on fossil fuels, makes it one of the most alarming responsible for the greenhouse effect. A wide range of measurements confirm that the atmospheric mixing ratio of CO_2 has increased by about 100 ppmv (36%) over the last 250 years, from a range of 275 to 285 ppmv in the pre-industrial era (AD 1000-1750) to 379 ppmv in 2005 and its average rate of increase is 1.4 ppmv yr^{-1} (IPCC 4th Assessment Report: Climate Change 2007).

Figure 3 shows the average tropospheric content of CO_2 (parts per million of volume, ppmv) over the Mediterranean basin during the month of July 2010. The field is smoothed with a low pass filter, which uses a pixel-wise adaptive Wiener filtering method based on statistics estimated from a local neighbourhood of each pixel, in order to emphasize the patterns.

From Figure 3 we can see that there is not a homogeneous distribution of CO_2 in the Mediterranean area. There is a clear north-westward gradient of the concentration which is overlapped by other small-scale features. In particular, there is a high concentration of the gas in the south-eastern part of the basin. From Figure 2 we can see that there are few available measurements in this area. This could lead us to the conclusion that what we see is the effect of a special event of high CO_2 concentration that could have occurred in that part of the basin and that a specular event could have occurred over the Black Sea during the month. This fact should be further investigated. Anyway, the available measurements in the middle of the basin are enough to affirm that there is a strong northward component of the gradient of a few (3-4) ppmv from the Tyrrhenian basin towards the Adriatic basin and that the same occurs in the Aegean Sea. Furthermore, this gradient is observed also at the ground stations. Table 2 shows the monthly averages at the stations and the monthly averages retrieved from IASI around the stations.

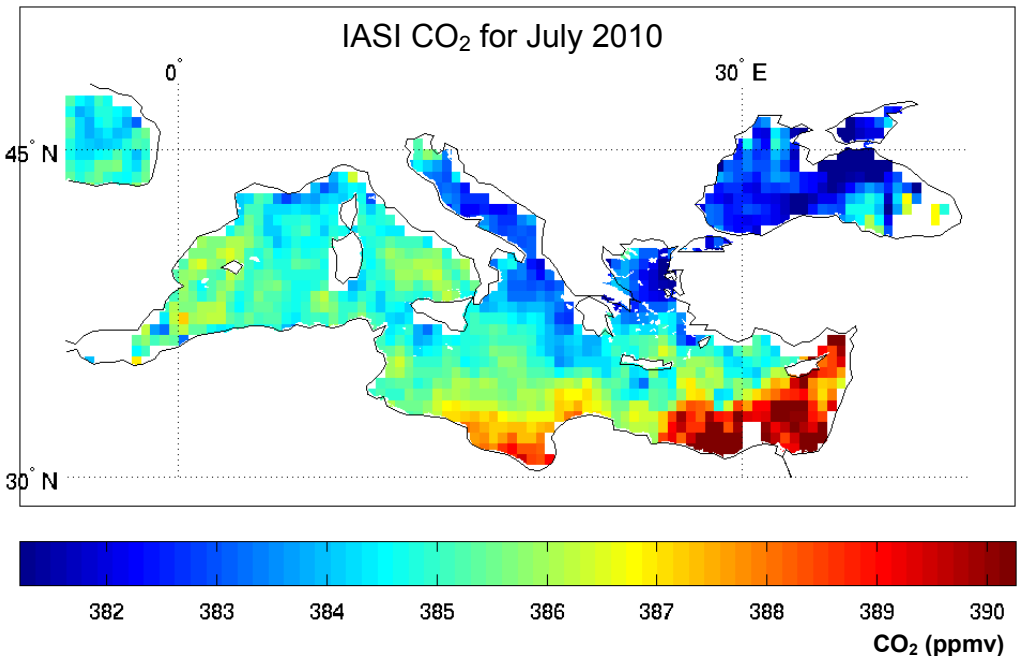

Figure 3: Monthly averages for CO_2 tropospheric content from IASI retrieval.

Table 2: Monthly averages from ground-based measurements and from IASI retrieval of CO_2 concentrations. The stations are ordered in a south-eastward direction.

Station	Ground measurements (ppmv)	IASI retrieval (ppmv)
Begur	385.67	382.49
Lampedusa	385.73	386.81
Finokalia	383.5	386.37
Cairo	386.8	392.06

The gradient is much more marked in the IASI retrieval than in the ground-based measurements but the trend is exactly the same. The local minimum observed in Finokalia is evident also in the IASI retrieved field (the small blue spot south of Crete Island). The physical reasons for this strong difference in the gradient magnitude may be due to the fact that the boundary layer is a turbulent part of the atmosphere. Therefore, the concentrations tend to be homogenized with respect to the free troposphere.

CH_4

Methane has the second largest RF of the long-lived greenhouse gases (from now on LLGHGs) after CO_2 (IPCC 4th Assessment Report: Climate Change 2007). In 2005, the global average abundance of CH_4 measured by the network of 40 surface air flask sampling sites operated by NOAA/GMD in both the hemispheres was 1,774.62 ± 1.22 ppbv, whilst the pre-industrial concentration estimated from ice core measurements was about 750 ± 4 ppbv in 1750. Its growth rate has decreased form 1% yr^{-1} in the late 1970s and early 1980s to zero by the end of the 1990s. The reasons for the decrease of the atmospheric CH_4 growth rate are not understood but are clearly related to changes in the imbalance between CH_4 sources and sinks. The sources of atmospheric CH_4 are mostly biogenic and include wetlands, rice agriculture, biomass burning and ruminant animals.

Methane is also emitted by various industrial sources including fossil fuel mining and distribution.

Figure 4 shows the monthly averaged CH_4 atmospheric concentration over the Mediterranean basin after the same filtering tool used for Figure 3.

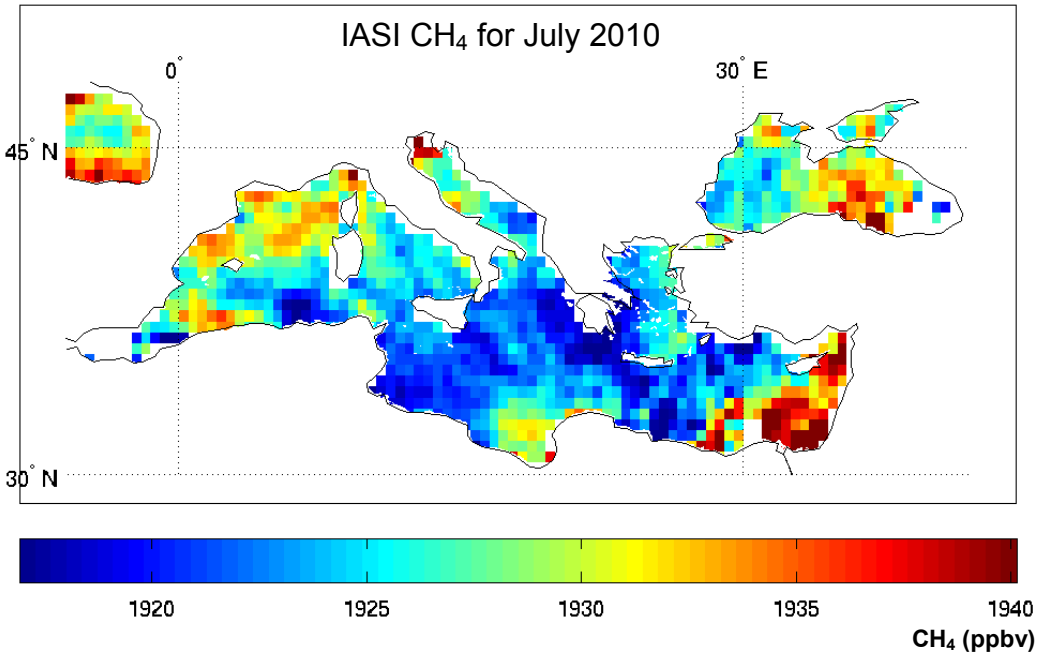

Figure 4: Monthly averages for CH_4 tropospheric content from IASI retrieval.

Figure 4 shows a different trend with respect to the CO_2 concentration. Here, it seems that we have rather a parabolic trend in the northwest-southeast direction. Once more we have to remark that the eastern part of the basin has few samples and this effect may be rather representative of a peak event. In the best sampled area we register a minimum in the Aegean Sea and a maximum in the Ligure-Provencal basin which partly extends over the Tyrrhenian Sea.

Table 3 shows the averaged ground measurements and the averaged retrieved values for the CH_4 concentrations on 4 of the 5 selected GAW stations.

The first evident feature is that the retrieved values are noticeably higher than the ground-based measurements. This feature is quite expected. It would be the same value if the profile was constant with altitude, but that is not the case. The retrieval is not sensible to the boundary layer and is instead representative of the tropospheric concentration of the gas.

On the other hand, the geographical trend is the same. Here, the situation is the opposite of the situation described for CO_2. The intensity of the gradient is much stronger for the ground measurements than for the retrieval. In fact, the retrieved values range in an interval of 20 ppbv, whilst the ground-based measurements range in an interval of more than 50 ppbv. As stated before, the Ligure-Provencal basin is an area of local maximum for the concentration of CH_4. Anyway, if we carefully look at Figure 4, the only small blue spot is exactly around Begur and this is confirmed also by ground-based measurements. This gives an idea of the performance of the retrieval from the point of view of the geographical resolution.

Table 3: Monthly averages from ground-based measurements and from IASI retrieval of CH_4 concentration. The stations are ordered in a south-eastward direction.

Station	Ground measurements (ppbv)	IASI retrieval (ppbv)
Begur	1833.95	1920.14
Lampedusa	1859.84	1923.56
Finokalia	1864.7	1930.13
Sede Boker	1889.65	1936.32

N_2O

N_2O is a powerful GHG with a lifetime of about 114 years. Its global warming potential (GWP) is 298 times higher than that of CO_2. Its mean mixing ratio in Lampedusa during 2008 was 322.5 ppbv and its annual growth rate is estimated to be 0.78 ppbv yr^{-1} with a linear trend. The agreement of recorded data in Lampedusa with the global data reported by the IPCC, 2007 makes this site a good proxy to monitor the concentration of N_2O on both global and regional scale (12).

It is the major source of NO to the stratosphere and with the considerable reduction of CFCs in the atmosphere thanks to the Montreal protocol, it is the dominant ozone-depleting substance emitted in the 21st century (13).

N_2O is produced both naturally and anthropogenically. The anthropogenic activity includes the use of ammonium fertilizers in agriculture, the fuel combustion, the adipic and nitric acid industrial production and waste management activities (14). The natural processes which influence the N_2O tropospheric concentration are of biological and abiotic nature. Natural microbial production accounts for about 2/3 of N_2O emissions. Among the abiotic processes, the seasonal ingassing and outgassing of cooling and warming surface waters create a thermal signal in the tropospheric N_2O (15).

Figure 5 shows the average N_2O tropospheric concentration for the month of July. The original field has been filtered with the Wiener filter exactly as done for CO_2 and for CH_4.

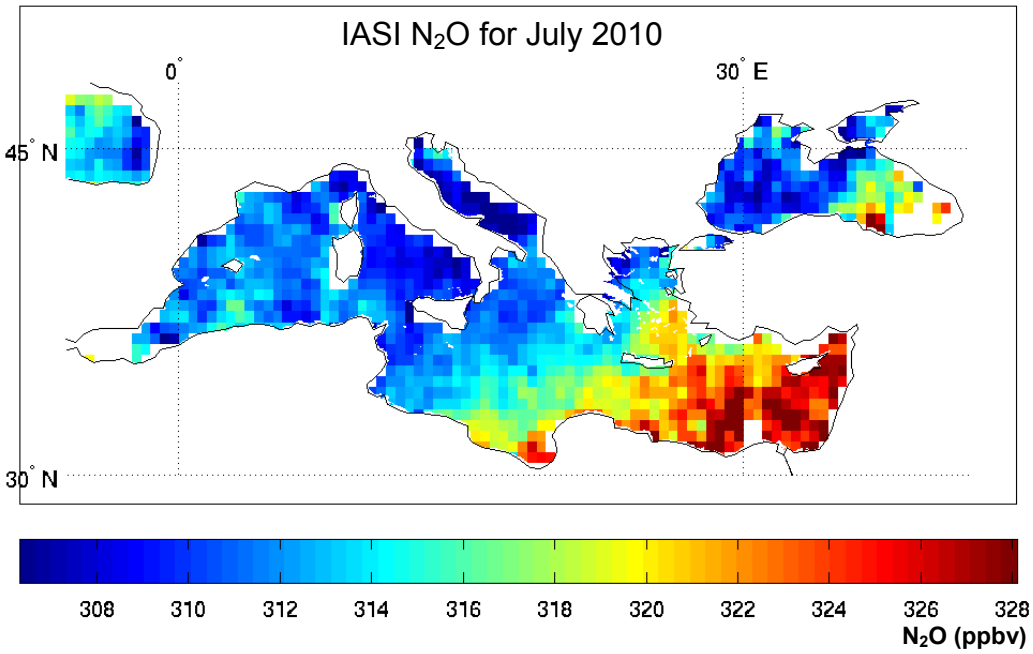

Figure 5: Monthly averages for N_2O tropospheric content from IASI retrieval.

Figure 5 shows a very well marked north-westward gradient which is partly in agreement with the CO_2 trend. Figures 3 to 5 confirm that the south-eastern part of the basin is the most polluted one. Once more we remark that the phenomenon may be caused by a down sampling of the area, but as in the case of CO_2 and CH_4, the N_2O gradient is confirmed also in the central part of the basin, where the available IASI measurements are copious.

The only station with available ground-based measurements is the ENEA station located in Lampedusa. The monthly averaged retrieved value is 309 ppbv, whilst the ground-based averaged measurement is 323 ppbv. This disagreement is expected, as in the case of all trace gases which do not have a constant vertical profile. The retrieval is sensible to the N_2O concentration between 800 and 200 hPa, therefore it misses all signals from the lowest atmospheric layers. We know that a higher concentration in the boundary layer with respect to the free troposphere is compatible with real observed data. Let us consider the following two figures (7 and 8). They show the distribution of aircraft N_2O concentration measurements at altitudes between 0 and 2000 m (corresponding to

approximately 800 hPa) and between 2000 and 8000 m (corresponding to approximately 200 hPa) on the area around Japan shown in Figure 6 from February 2011 to February 2013 (data acquired by the Japanese Meteorological Agency). The average values of the two distributions are 320 ppbv and 314.8 ppbv, respectively.

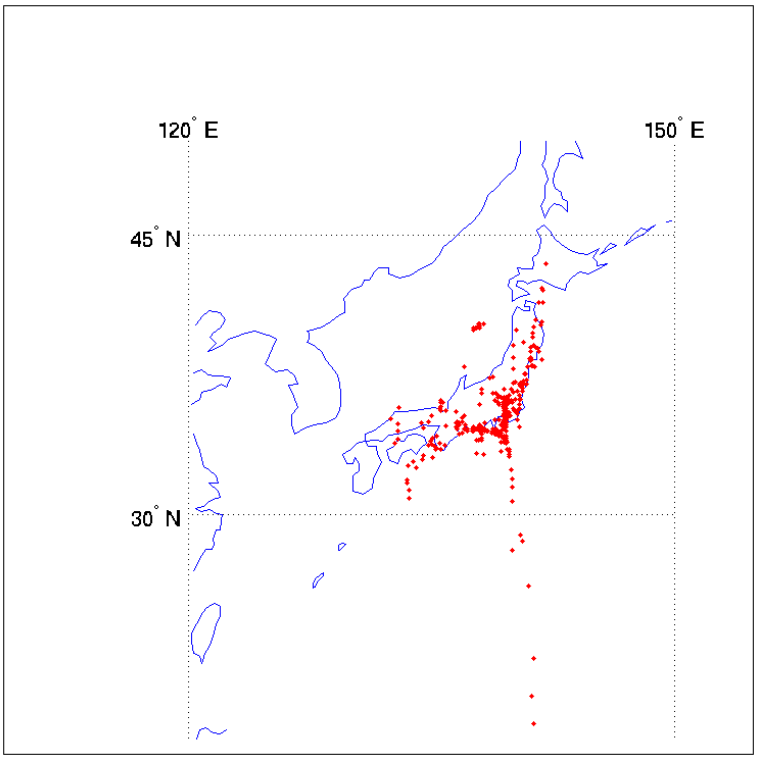

Figure 6: Airplane geographic position during the acquisition of N_2O samples from February 2011 to February 2013 (http://ds.data.jma.go.jp/gmd/wdcgg/wdcgg.html).

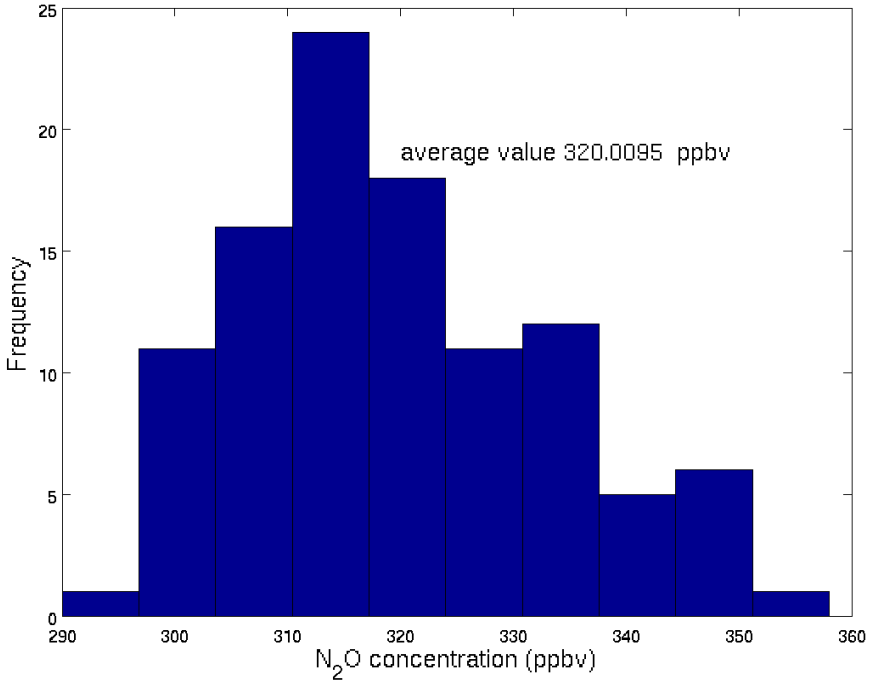

Figure 7: Distribution of aircraft measurements at altitudes between 0 and 2000 m on an area around Japan between February 2011 and February 2013 (http://ds.data.jma.go.jp/gmd/wdcgg/wdcgg.html).

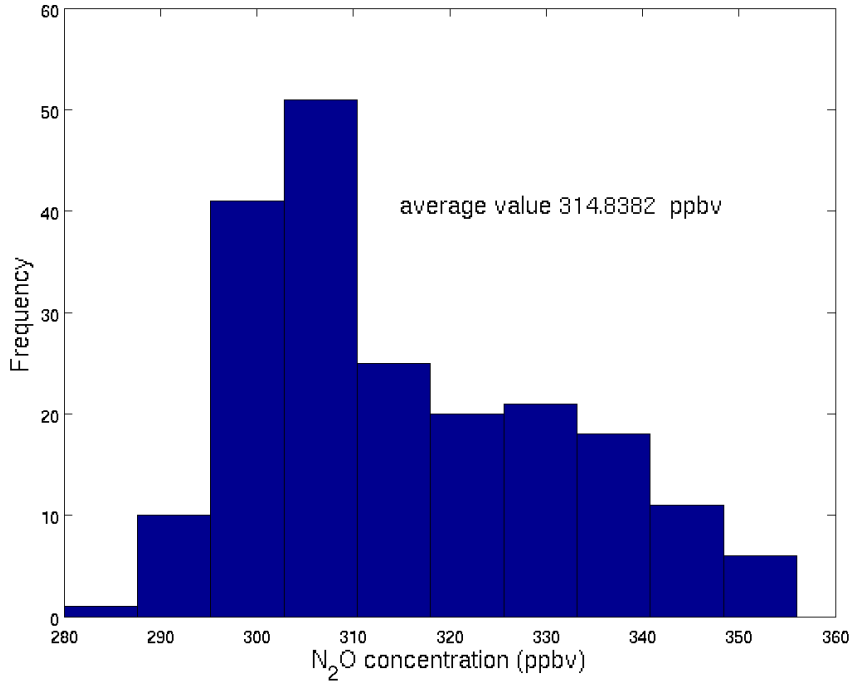

Figure 8: Distribution of aircraft measurements at altitudes between 2000 and 8000 m on an area around Japan between February 2011 and February 2013 (http://ds.data.jma.go.jp/gmd/wdcgg/wdcgg.html).

We want to remark that this comparison is not aimed at demonstrating that the free tropospheric concentration of N_2O on the Mediterranean area is lower than the boundary layer concentration. It is aimed simply at showing that kind of this vertical distribution of N_2O concentration is realistic. At the same time, we do not dispose of a statistically significant time series of measurements in the area of Japan in order to affirm that this is an average natural trend and that this trend is the same in the Mediterranean basin.

It is important to stress that most atmospheric sources of N_2O are located at the surface. As previously stated, the biological emission of N_2O accounts for 2/3 of the total emissions and all anthropogenic sources are also located at the surface. Therefore, it is plausible that the concentration of N_2O is higher at the surface than in the rest of the troposphere, where part of the gas is destroyed.

CO

CO is not considered a proper greenhouse gas, but it has a strong indirect influence on the atmospheric radiative balance. The most important sources of CO are biomass burning and fossil fuel combustion. Almost half of the total burden of CO comes from the oxidation of CH_4 and non-methane hydrocarbons (NMHC), like isoprene. Vegetation and oceans are considered to be sources of secondary importance. On the other side, around 90% of CO is destroyed by reaction with the hydroxyl (OH) radical and the remaining 10% is captured by soils (16). CO has a strong influence on the lifetimes of LLGHG because of its reaction with OH. Furthermore, CO and CH_4 oxidation is partially responsible for the production and destruction of tropospheric ozone. It has a lifetime of 1-2 months and is therefore considered a good tracer to study the tropospheric transport of pollution (17).

Figure 9 shows the monthly average of CO concentration over the Mediterranean basin for the month of July after the application of a low pass filtering tool as done for the other trace gases we previously dealt with.

The monthly averaged CO field has characteristics similar to the other averaged trace gas fields (Figures 3, 4 and 5). The westward gradient of CO concentration is very well marked. The absolute maximum is located in the south-eastern part of the basin, as for the other trace gases, but a local maximum is well distinguishable in the Ligure-Provencal basin. Once more, we cannot be sure of the high concentration recorded in the extreme eastern part of the basin because of the low

amount of available satellite measurements, but the gradient is the same (both in direction and intensity) in the better sampled central area of the basin.

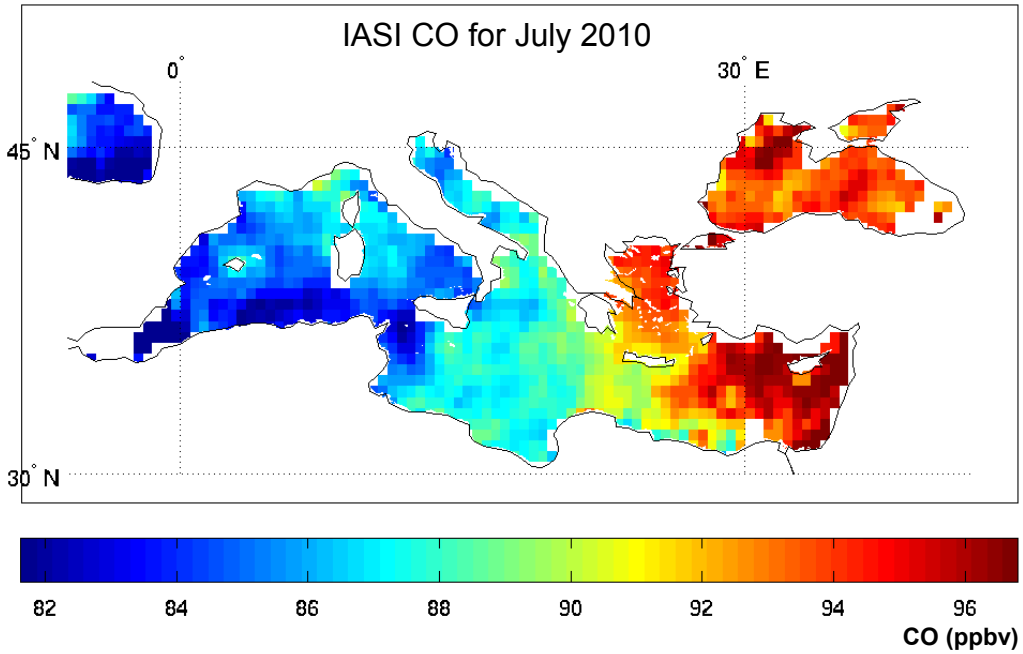

Figure 9: Monthly averages for CO tropospheric content from IASI retrieval.

The monthly averaged retrieved concentration is 85 ppbv in Lampedusa and 96 ppbv in Sede Boker, where the monthly averaged ground measurements are 121 and 140 ppbv, respectively. The difference is around 40 ppbv for both stations. This large difference is due to the fact that the retrieved values refer to the tropospheric content of the gas (atmosphere between 700-800 and 200 hPa). This difference is expected, because we do not expect the vertical profile of CO to be constant with altitude. The experimental measurements acquired by the MOZAIC (Measurements of OZone water vapour, carbon monoxide and nitrogen oxides by in-service AIrbus airCraft) experiment confirm this trend. Klonecky et al. 2012 (18) concentrate their analysis on the period from May to December 2008 mainly in the north Atlantic area. They show that CO has a monthly average concentration of around 130 ppbv in the atmospheric layers between 1050 and 800 hPa and a concentration of around 90-100 ppbv in the layers between 800 and 300 hPa, the part of the atmosphere where IASI data have best sensitivity. The difference is around 30 ppbv and is consistent with the differences that we found in our comparison.

The gradient observed from the retrieved CO concentration seems to be supported by the ground measurements. This fact seems to confirm once more that the eastern part of the Mediterranean works as a collector or a source of pollution. The reasons for this feature should be investigated and go beyond the purposes of this study, but the first impression is that it could be due to the presence of large metropolitan and polluted areas like Cairo and Istanbul supported by a general circulation which does not allow the replacement of polluted air with new fresh air. This thesis is supported by a fast look at the brightness temperature frames acquired in the infrared channel at 12 μm by the imaging radiometer SEVIRI onboard the geostationary platform Meteosat Second Generation for the whole month of July 2010. From these frames it can be seen that the Eastern Mediterranean is often affected by a local high-pressure condition associated with a flux from Central and Eastern Europe. Kalabokas et al. 2013 (19) show that the highest tropospheric ozone levels recorded in the Eastern Mediterranean occur under high-pressure (anticyclonic) meteorological conditions. These meteorological conditions are also associated with a lower troposphere and boundary layer flow transporting pollutants from Central and Eastern Europe and/or the Balkans towards the Eastern Mediterranean.

Time performance of the code

The down-sampling of the layer optical depth database has given a considerable speed-up to the code. Consider that for applications related to IASI, the layer optical depth database has reduced from 2 Gb to 0.5 Gb. Table 4 shows the performance of the code evaluated on a dedicated machine equipped with 6 physical and 6 virtual intel i7 cores with a clock frequency of the clock processor unit (CPU) of 3.33 GHz and a total RAM memory of 24 Gb.

Table 4: Time performance of the code expressed in seconds evaluated on the whole IASI spectral range (645-2760 cm^{-1}). FR stands for full resolution layer optical depth database, LR stands for the low resolution one, R stands for spectral radiance, JT for Jacobian of temperature, JTS for Jacobian of skin temperature, JH_2O for Jacobian of water vapour, JO_3 for Jacobian of ozone. ALL stands for all the entities which can be calculated by the code. Apart from R, JT, JH_2O, JTS and JO_3, it includes also the Jacobian of N_2O, the Jacobian of CO_2, the Jacobian of CO, the Jacobian of methane, the Jacobian of all not modifiable mixed gases and the three Jacobians of continua coefficients, the self and foreign ones for water vapour and the foreign one for CO_2.

	FR (s)	LR (s)	Speed-up
R	15	.95	15.8
R, JTS, JT, JH_2O, JO_3	41	3.5	11.7
ALL	103	9.3	11.1

The performance has been evaluated on the whole IASI spectral range (645-2760 cm^{-1}) in three different cases which we think are more representative of the possible applications. The first refers to the simple computation of the radiance spectrum, the second is referred to the computation of the spectral radiance and of the Jacobians of skin temperature, temperature, water vapour and ozone profiles and finally, the case where all the possible entities the code can compute are definitely computed. In addition to what was stated before, the code can compute the Jacobians of CO_2, CO, CH_4, N_2O, mixed not modifiable gases and self and foreign continua coefficients of water vapour and foreign continuum coefficient of CO_2. For all three combinations proposed in Table 4, the speed-up is always greater than 10. Furthermore, in absolute terms, the time performance of the new code makes it useful also for operational purposes. Just to have an idea, the average time spent per inversion is around 14 s. In particular, when the number of iterations is just one, the time decreases to around 8 seconds.

This result suggests the conclusion that a good choice of the first guess considerably reduces the computational time. This time seems still too much for operational purposes, if we consider that a sensor like IASI acquires around 90000 spectra per orbit in a time interval of around 1h40m. This means that each spectrum is acquired in around 0.1 second and this would seem the reference time for operational purposes. Anyway, not all the acquired spectra may be processed by the inverse radiative transfer tool described in (3). In fact, this method can be applied to only clear sky spectra. As a thumb rule, the clear sky spectra on the whole hemisphere are around 20-30% of the total. If we consider 10 seconds as the average time to retrieve the thermal and humidity state of the atmosphere, a cluster of 50 CPUs like the one used in this application is enough for operational purposes. The use of a physical based methodology to retrieve the thermal and humidity state of the atmosphere would considerably increase the quality of the level 2 products.

The factors responsible for this speed-up may seem obvious but it is worth discussing them briefly. The fact that the size of the layer optical depth database is reduced by a factor 4 has multiple implications on the performance of the code. In fact, the first conclusion is that the code makes much less floating point operations. Furthermore, the small size of the new down-sampled database makes it possible to store all the parameterized optical depth coefficients in the RAM memory. This allows a more efficient use of the input/output operations with a consequent reduction of the operating system calls and of the interruption of the CPU pipeline.

CONCLUSIONS

A new implementation of the σ-IASI code has been presented. The layer optical depth database has been down-sampled and this allows an operational use of the code in order to retrieve the thermodynamic state of the atmosphere and the tropospheric concentration of the trace gases CO, CO_2, CH_4 and N_2O. An application of the code has been proposed: the tropospheric concentration (800-200 hPa) of the above-mentioned trace gases has been retrieved for the month of July 2010 by means of a retrieval scheme based on the FTS-PSI technique and the results have been discussed and compared to the ground-based measurements coming from the GAW stations in the Mediterranean Basin. The comparison shows that the retrieval is compatible with the typical vertical profiles of the trace gases studied.

The monthly averaged fields show that the eastern part of the Mediterranean Basin has a higher concentration of pollutants with respect to the western part. The physical causes of this phenomenon have to be further investigated, but the first impression is that the Mediterranean atmospheric circulation in that period of the year brings pollutants generated by the metropolitan areas of Cairo, Istanbul as well as in Central and Eastern Europe and in the Balkans towards the eastern part of the basin and does not allow a renewal with fresh air.

ACKNOWLEDGEMENTS

The ground-based measurements in Lampedusa and Sede Boker have been provided by NOAA/ESRL and have been downloaded from http://www.esrl.noaa.gov/gmd/dv/iadv/. The ground-based measurements in Begur and Finokalia have been provided by Laboratoire des Sciences du Climat et de l'Environnement (http://www.lsce.ipsl.fr/). The ground-based measurements in Cairo have been provided by the Egyptian Meteorological Authority (http://ema.gov.eg/). The ground-based measurements of N_2O in Lampedusa have been provided by the Italian Agency ENEA. The N_2O vertical profiles acquired by mobile aircraft platform have been provided by the Japanese Meteorological Agency and have been downloaded from the WDCGG website http://ds.data.jma.go.jp/gmd/wdcgg/wdcgg.html.

REFERENCES

1 Aumann HH, M T Chahine, C Gautier, M D Goldberg, E Kalnay, L M McMillin, H Revercomb, P W Rosenkranz, W L Smith, D H Staelin, L L Strow, & J Susskind, 2003. Airs/amsu/hsb on the aqua mission: design, science objectives, data products, and processing systems. IEEE Transactions on Geoscience and Remote Sensing, 41(2): 253-264

2 Cayla F-R, 1993. IASI infrared interferometer for operations and research. In: High Spectral Resolution Infrared Remote Sensing for Earth's Weather and Climate Studies, 9-19. Edited by A Chedin, MT Chahine & N A Scott, NATO ASI Series I Global Environmental Change Vol. 9 (Springer, Berlin-Heidelberg) 306 pp.

3 Masiello G, C Serio, A Carissimo, G Grieco & M Matricardi, 2009. Application of φ-IASI to IASI: Retrieval products evaluation and radiative transfer consistency. Atmospheric Chemistry and Physics, 9(22): 8771-8783

4 Amato U, G Masiello, C Serio & M Viggiano, 2002. The σ-IASI code for the calculation of infrared atmospheric radiance and its derivates. Environmental Modelling & Software, 17/7: 651-667

5 Masiello G & C Serio, 2003. An effective water vapor self-broadening scheme for look-up-table-based radiative transfer. In: Society of Photo-Optical Instrumentation Engineers (SPIE) Conference Series. Vol. 4882, edited by K P Schaefer, O Lado-Bordowsky, A Comeron & R H Picard, 52-61

6 Shepard M, S A Clough, M J Iacono & J L Moncet, 1992. Line-by-line calculations of atmospheric fluxes and cooling rates: Application to water vapor. Journal of Geophysical Research: Atmospheres, 97(D14): 15761-15785

7 Anderson G P, S A Clough, F X Kneizys, J H Chetwynd & E P Shettle, 1986. AFGL atmospheric constituent profiles (0-120 km). Rep. *AFGL*-TR-86-0110 (Air Force Geophysics Laboratory, Hanscom AFB, MA 01736, USA)

8 Rothman L S, I E Gordon, A Barbe, D C Benner, P F Bernath, M Birk, V Boudon, L R Brown, A Campargue, J P Champion, K Chance, L H Coudert, V Dana, V M Devi, S Fally, J M Flaud, R R Gamache, A Goldman, D Jacquemart, I Kleiner, N Lacome, W J Lafferty, J Y Mandin, S T Massie, S N Mikhailenko, C E Miller, N Moazzen-Ahmadi, O V Naumenko, A V Nikitin, J Orphal, V I Perevalov, A Perrin, A Predoi-Cross, C P Rinsland, M Rotger, M Simeckova, M A H Smith, K Sung, S A Tashkun, J Tennyson, R A Toth, A C Vandaele & J Vander Auwera, 2009. The HITRAN 2008 molecular spectroscopic database. Journal of Quantitative Spectroscopy & Radiative Transfer, 110(2009): 533-572

9 Grieco G, G Masiello, C Serio, R L Jones & M I Mead, 2011. Infrared atmospheric sounding interferometer correlation interferometry for the retrieval of atmospheric gases: the case of H_2O and CO_2. Applied Optics, 50: 4516-4528

10 Grieco G, G Masiello & C Serio, 2010. Interferometric vs spectral IASI radiances: Effective data-reduction approaches for the satellite sounding of atmospheric thermodynamical parameters. Remote Sensing, 2: 2323-2346

11 Lubrano A M, G Masiello, M Matricardi, C Serio & V Cuomo, 2004. Retrieving N_2O from nadir-viewing infrared spectrometers. Tellus, Series B, Chemical and Physical Meteorology, 56(3): 249-261

12 Artuso F, P Chamard, S Chiavarini, A di Sarra, D Meloni, S Piacentino & M D Sferlazzo, 2010. Tropospheric halocompounds and nitrous oxide monitored at a remote site in the Mediterranean. Atmospheric Environment, 44(38): 4944-4953

13 Ravishankara A R, Daniel J S & Portmann R V, 2009. Nitrous oxide (n2o): The dominant ozone-depleting substance emitted in the 21st century. Science, 326: 123-125

14 Cicerone R J, 1989. Analysis of sources and sinks of atmospheric nitrous oxide (N_2O). Journal of Geophysical Research: Atmospheres, 94(D15): 18265-18271

15 Nevison C D, E Dlugokencky, G Dutton, J W Elkins, P Fraser, B Hall, P B Krummel, R L Langenfelds, S O'Doherty, R G Prinn, L P Steele & R F Weiss, 2011. Exploring causes of interannual variability in the seasonal cycles of tropospheric nitrous oxide. Atmospheric Chemistry and Physics, 11(8): 3713-3730

16 Brenninkmeijer C A M & P C Novelli, 2003. Encyclopedia of Atmospheric Sciences, 1st edition, Volume 1 (Academic Press, London, UK) 2389-2396

17 Logan J A, M J Prather, S C Wofsy & M B McElroy, 1981. Tropospheric chemistry: A global perspective. Journal of Geophysical Research: Oceans, 86(C8): 7210-7254

18 Klonecki A, M Pommier, C Clerbaux, G Ancellet, J P Cammas, P F Coheur, A Cozic, G S Diskin, J Hadji-Lazaro, D A Hauglustaine, D Hurtmans, B Khattatov, J F Lamarque, K S Law, P Nedelec, J D Paris, J R Podolske, P Prunet, H Schlager, S Szopa & S Turquety, 2012. Assimilation of IASI satellite CO fields into a global chemistry transport model for validation against aircraft measurements. Atmospheric Chemistry and Physics, 12(10): 4493-4512

19 P D Kalabokas, J P Cammas, V Thouret, A Volz-Thomas, D Boulanger & C C Repapis, 2013. Examination of the atmospheric conditions associated with high and low summer ozone levels in the lower troposphere over the eastern Mediterranean. Atmospheric Chemistry and Physics, 13: 10339-10352